Chapter 3

Effect of Background Turbulence on Animal-Fluid Transport

3.1 Introduction

Medusae are known to be voracious predators capable of impacting pelagic communities [85]. Most species capable of exerting a high predatory impact forage as cruising predators [24]. Cruising medusae are effective predators as a consequence of their high population densities and the mechanics of their feeding, which enable very high, non-satiating feeding rates [22, 102, 129]. Since cruising medusae use swimming motions to feed [86, 21, 22], their fluid interactions during swimming need to be quantified to understand the mechanics of their feeding and to predict how morphology and swimming behavior may influence their predatory impact.

Cruising medusae rhythmically contract and relax their bells in order to swim. In addition to providing thrust, this bell motion transports fluid to prey capture surfaces (i.e., tentacles and manubrium/oral arms) where entrained prey may be captured [22, 19, 96]. The fluid interactions and patterns of flow around swimming, cruising medusae have been well described qualitatively [103, 19, 28]. These studies have shown that as the bell expands, fluid adjacent to the bell margin is entrained and drawn through trailing tentacles into a stopping vortex ring that rotates inside the subumbrellar cavity. As the bell contracts, fluid continues to be entrained adjacent to the bell margin and, along with fluid from the stopping vortex, is drawn into a starting vortex ring that rotates through the trailing tentacles in the wake of the medusae. Consequently, fluid appears to be

continuously entrained throughout the swimming cycle and interacts with capture surfaces [28].

While these studies have provided a general understanding of how water is transported near the bell and in the wake of cruising medusae, they have provided less in terms of quantitatively characterizing fluid transport. Few studies have attempted to quantify the flow around medusae [113, 96], yet modeling and prediction of ingestion and prey selection by cruising medusae requires a quantitative description of how these medusae entrain fluid while swimming. Characteristics of fluid transport affect feeding by determining the amount and types of prey entrained and encountered. Encounter rates (defined here as the number of prey that enter the capture zone over time) are controlled by the amount of fluid that is entrained and transported past capture surfaces over time. The type and amount of prey entrained will largely be determined by prey characteristics such as size, swimming speed and reactivity [49, 134, 122] in relation to fluid characteristics such as flow velocities and deformation rates [47, 69, 12]. These important fluid parameters have yet to be quantified in detail for medusae.

Quantitative studies of flow surrounding swimming animals have been conducted in the past and utilize techniques that include digital particle image velocimetry (DPIV; [133, 131]). Laboratory settings are necessary for pragmatic reasons and enable high-quality detailed descriptions of animal-fluid interactions. However, the relevance of these descriptions in field conditions is generally unknown. For medusae, qualitative flow visualizations conducted in the laboratory that identified important fluid structures around medusae (e.g., stopping and starting vortices; [22, 18, 103]) have been shown to be relevant in the field [30, 19]. However, the quantitative characteristics of flow around medusae are likely to be altered by natural flow and turbulence conditions [69]. For this reason, it is important to develop approaches that can be used to evaluate the impact of natural flow patterns on fluid processes governing predator-prey interactions.

Our approach towards reaching that goal was to use an analysis tool called Lagrangian coherent structures (LCS) derived from DPIV data [52, 115, 113] to quantify the fluid interactions of swimming medusae. While conventional DPIV analysis computes velocity vector fields that can be used to estimate fluid energetics and identify fluid structures such as vortex rings [113], LCS analysis expands

the utility of conventional DPIV by increasing our ability to describe and quantify feeding-related fluid transport around swimming medusae. Here we describe these patterns for the cruising-foraging leptomedusa, *Aequorea victoria*. Members of the genus *Aequorea* are distributed throughout the world's oceans and have been demonstrated to be influential predators on a range of zooplankton, including fish eggs and larvae [99, 100, 23]. The recent extension of DPIV techniques from the laboratory to in situ conditions using a self-contained underwater velocimetry apparatus (SCUVA; [66]) enables us to compare the laboratory results with a field data set.

3.2 Methods

3.2.1 Experimental Methods

Measurements of capture efficiency were conducted at Marine Biological Laboratory (Woods Hole, MA). *Aequorea victoria* were acquired from the New England Aquarium (Boston, MA) and held in containers for acclimation to room temperature before measurements. Four species of prey were used in this study: *Artemia salina*, adult *Acartia tonsa*, juvenile *Mnemiopsis leidyi*, and *Libinia emarginata* eggs. These prey were chosen to compare the effects of hard- or soft-bodied prey, prey size and escape behavior on capture by *Aequorea victoria*. *Artemia salina* were cultured in the lab from dehydrated cysts (Connecticut Valley Biological Supply); *Acartia tonsa* and *Mnemiopsis leidyi* were collected using standard plankton net tows in Woods Hole, MA. Eggs of *Libinia emarginata* were harvested from live females collected off the coast of Woods Hole, MA. Rectangular filming vessels were filled with filtered seawater and medusae were placed in the vessel with a monoculture of prey. Interactions between medusae and prey were filmed and quantified from 30 hours of video with 23 medusae, yielding 214 encounters. Encounters (defined as an event where prey is entrained in the medusae wake and passes through its tentacles) and captures (an event where prey is encountered and adheres to a medusa's tentacles for more than 2 s) were quantified from the video footage. Finally, the capture efficiency was found by taking the ratio between number of prey captured and number of prey encountered.

Quantitative flow measurements in the laboratory and the field were conducted at Friday Harbor Laboratories in Friday Harbor, WA. Animals were collected off the Friday Harbor Laboratory dock and acclimated to room temperature before conducting laboratory measurements. In the laboratory, *Aequorea victoria* specimens approximately 5 cm in diameter were placed in large glass filming vessels with dimensions several body lengths greater than the medusae in order to minimize vessel artifacts in the flow. The aquarium was filled with natural, unfiltered seawater. Seawater that was used in the aquarium contained sufficient suspended particulate to enable quantitative visualization. Fluorescent dye was used to qualitatively describe the fluid structures generated by a swimming animal. The flow field was quantitatively measured in the laboratory and field using digital particle image velocimetry (DPIV; [140]). Components for DPIV experiments often include a laser (for flow illumination), optics (designed to spread laser beam into a thin sheet to illuminate a plane in the flow), a camera to record consecutive images, and a software package that uses a cross-correlation scheme to analyze particle displacements and output velocity fields. The flow field was illuminated by a single 350 mW, 532 nm solid-state laser with optics that created a sheet less than 2 mm thick. A video camera (Sony HDR-FX1) was oriented perpendicular to the light sheet and captured images in the laser plane at pixel resolution and a frame rate of 30 s^{-1}. Measurements in the field were accomplished by using a self-contained underwater velocimetry apparatus (SCUVA; [66]), which used the same laser and video camera as described for the laboratory. Only sequences where the laser sheet remained in the center of the medusae were used for analysis. Laser sheet alignment through the center of the animal body was identified when the manubrium (centrally located in the subumbrellar cavity) was fully illuminated.

In the laboratory, five *Aequorea victoria* were videotaped while swimming for multiple pulse cycles through the laser-illuminated field of view. Additionally, a single data set with multiple swimming cycles (necessary for the LCS analysis) was obtained in situ. Based on the location of the laser sheet relative to the camera, a conversion ratio of 26 pixels cm^{-1} (laboratory) and 45 pixels cm^{-1} (field) was used for subsequent DPIV analysis. Each image was evaluated with an interrogation window size of 16×16 pixels and a 50% overlap. Calculations of velocity and vorticity

fields possess an uncertainty of 5% and 7%, respectively (based on propagating error associated with the camera-laser system). The DPIV analysis produced velocity field data every 0.033 s over a domain approximately 18×28 cm^2 in the laboratory and 10×16 cm^2 in the field. This velocity data was used to compute the flow map for the LCS analysis. For this experiment, long integration time T corresponds to 60 frames of data (or $|T| = 60$ frames) and short integration time correspond to $|T| = 30$ frames. Velocity vectors for the field data have been corrected for diver motion by subtracting the mean flow, which is computed by averaging the components of velocity in the x- and y-direction from the entire velocity field [66]. Maximum animal diameter and average distance traveled per swimming cycle were determined from consecutive video images. To avoid erroneous vectors due to animal body motion, the body outline was identified by thresholding the intensity of the images; any vectors located within the animal body were set to zero. The two-dimensional vorticity (ω) and total shear rate (τ) were found directly from DPIV velocity fields using [6]

$$\begin{aligned} \omega &= \frac{du}{dy} - \frac{dv}{dx}, \\ \tau &= \frac{du}{dy} + \frac{dv}{dx}. \end{aligned} \tag{3.1}$$

3.2.2 Lagrangian Method

Lagrangian coherent structures (LCS) are regions in a flow where maximum separation between adjacent packets of fluid occurs. For this reason, LCS are used to distinguish regions of differing dynamics found in turbulence [50], vortex rings [113, 105], and animal wakes [113, 95]. Because maximum divergence of particles will indicate LCS, the objective of the analysis is to find a measure of maximum particle separation over some integration time T during which the flow is observed. The quantity that measures particle separation is called the finite-time Lyapunov exponent (FTLE, [115]; or direct Lyapunov exponent field, [52]). Given an empirically-produced flow, the displacement of adjacent particles at time t_0 (initially separated by a distance $\delta x\,(t_0)$) and the final displacement of the same particle pair (denoted as $\delta x\,(t_0 + T)$), the finite-time Lyapunov exponent (σ) can be

defined as

$$\sigma_{t_0}^{T}(x) = \frac{1}{|T|} ln \left|\left| \frac{\delta x(t_0 + T)}{\delta x(t_0)} \right|\right|. \tag{3.2}$$

The FTLE is evaluated for each particle pair from equation (3.2), which results in a scalar field in the fluid of interest. Using the FTLE field that measures particle separation, the LCS can be determined from the hyperbolic ridges or local maxima of FTLE in the flow [52, 53, 115].

Consider the black curves in figure 3.1 that correspond to LCS with differing behavior. Two particles are initially close together and are located on either side of the LCS curve (figure 3.1, left). As time is advected forward, these two particles remain on either side of the LCS and their particle paths diverge (dashed, gray curves). This LCS, which is found by using positive integration time ($T > 0$ or forward-time), is formally called the repelling LCS. A second type of LCS can be found by using a negative integration time ($T < 0$ or backward-time), and these are attracting LCS. Two particles are initially far from each other and are located on either side of an attracting LCS (figure 3.1, right). As time is advected forward, the paths of the same particle pair converge. By combining the forward- and backward-time LCS curves, structures such as vortex rings and recirculation regions can be identified [105, 113, 48]. Larger integration time T increases spatial resolution of the LCS, however the choice of T is limited by the availability of data and computational costs.

In the case of field measurements where the measured flows are often dominated by regions of high shear, ridges in the FTLE field will indicate either material lines of high shear or the attracting and repelling LCS. Therefore, in order to isolate LCS curves from lines of high shear, the LCS curves were extracted from the FTLE fields using the criteria of Mathur et al. [84]. By thresholding or filtering the FTLE field, points surrounding a ridge of FTLE are identified. Once these points are known, the gradients of the FTLE scalar field are followed to the FTLE ridge, also known as gradient climbing. Gradient climbing will stop once conditions for a ridge location are met (i.e., Hessian matrix of FTLE has a negative eigenvalue and the angle between the FTLE gradient and the eigenvector corresponding to smaller-in-norm eigenvalue of Hessian shows no appreciable change). Finally, the hyperbolicity of a FTLE ridge is confirmed by using the rate of strain tensor of the flow

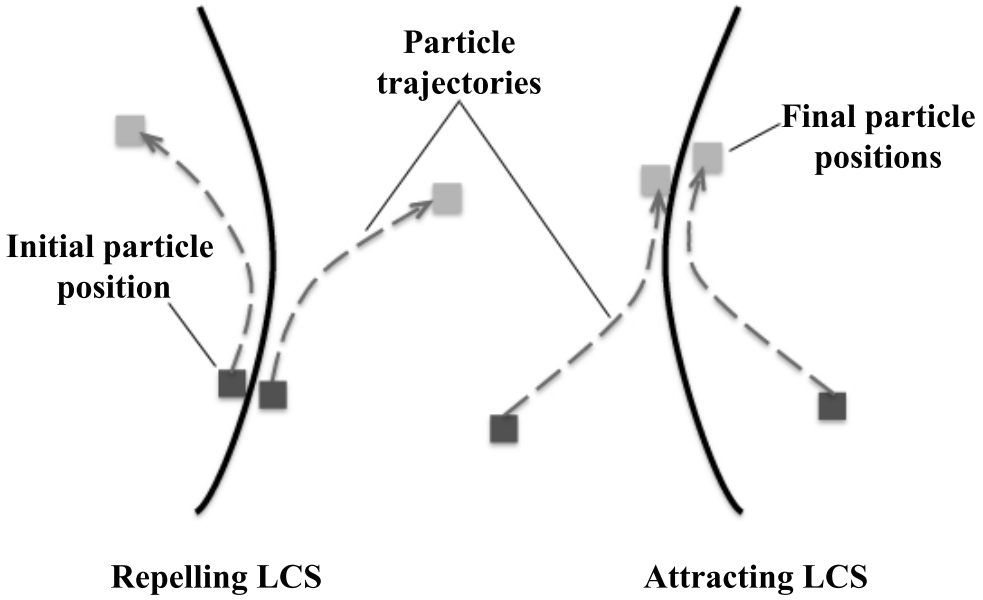

Figure 3.1. Behavior of particles near Lagrangian coherent structure (LCS) curves. As time is advected forward, the position of two initially adjacent particles on either side of a repelling LCS will diverge (left). For two particles initially on either side of an attracting LCS (right), as time is advected forward their positions converge to the attracting LCS curve. Solid black curves are LCS curves; dashed gray curves are particle trajectories with arrows indicating direction; dark and light gray boxes correspond to initial and final particle positions, respectively.

field [53]. The algorithms used to extract LCS from FTLE fields are explained in more detail by Dabiri and collaborators [95, 91].

In studies utilizing the LCS analysis, upstream LCS lobes identify regions in the fluid that become entrained by swimming medusae [113, 96]. Therefore, by measuring the shape and size of LCS lobes upstream of a swimming animal, we can quantify the volume of fluid that will be encountered by tentacles. Consequently, since each upstream LCS lobe corresponds to a single swimming cycle, the volume of an LCS lobe indicates the volume of fluid entrained by the animal per swimming cycle. Since the LCS analysis yields lobe areas (from a two-dimensional data set), the fluid entrainment volume per pulse is found by assuming radial symmetry of the upstream LCS lobes and revolving the area about the animal body's axis. Clearance rates were determined from the ratio of upstream LCS lobe volume and duration of a swimming cycle. Laboratory results are based on five different data sets with multiple swimming cycles; field values are based on a single data set with three consecutive swimming cycles. All analyses requiring the quantification of LCS utilize an integration time of $|T| = 30$ frames.

3.3 Results

3.3.1 Capture Efficiency Measurements

Prey tracks from the laboratory data are used to illustrate the location of entrained or encountered prey relative to the animal body (figure 3.2). Not all prey located upstream of the swimming animal are encountered (green tracks), which is indicative of discrete fluid regions that are later entrained into the animal's wake, confirming previous studies [113, 96]. These discrete packets of fluid are later transported into the vortex ring wake of the animal, which passes through downstream tentacles. Of those prey that were entrained or encountered, the number of prey that were captured by *Aequorea's* tentacles are then used to determine the capture efficiency (table 3.1). Data on encounter rate were not collected for each prey type and therefore not presented here, however the LCS analysis will provide encounter rate estimates from fluid dynamical quantities. Capture efficiency data collected

for *Aequorea victoria* (figure 3.3) are consistent with prey selectivity studies that links soft-bodied prey to high capture and retention efficiencies [100, 23].

Table 3.1. Summary of prey capture efficiency measurements for *Aequorea victoria* (data for *Libinia emarginata* body sizes were acquired from Costello and Henley [20]).

Prey type	Number of medusae	Body size (mm)	Capture efficiency
Libinia emarginata	5	1	0.82 ± 0.17
Mnemiopsis leidyi	4	11.5 ± 5.0	0.97 ± 0.06
Acartia tonsa	7	1.1 ± 0.1	0.37 ± 0.31
Artemia salina	5	0.7 ± 0.2	0.58 ± 0.08

3.3.2 Flow Visualization and Digital Particle Image Velocimetry

During a single swimming cycle, two vortex ring structures are visualized by fluorescent dye (figure 3.4). During bell contraction (figure 3.4A), a starting vortex is formed in the wake of *Aequorea victoria*. During bell relaxation (figure 3.4B), a stopping vortex is formed inside the subumbrellar cavity. A time series of velocity fields in the laboratory reference frame demonstrate that maximum fluid velocities are found within these vortices (indicated by red arrows) and areas adjacent to the bell margin (figure 3.5A). Shear fields calculated from the velocity vectors show that the vortices are also associated with the highest levels of shear around swimming *Aequorea victoria* (figure 3.6A and 3.6B).

The flow was measured around four other similarly-sized *Aequorea victoria* and the vector fields (not shown here) demonstrate that their fluid structures (i.e., generation of starting and stopping vortices) were similar to the medusae described in figures 3.5 and 3.6A. Combining the DPIV and LCS techniques, we were able to quantify marginal velocities and entrainment volumes (summarized in table 3.2). Maximum quantities in areas adjacent to the bell margin are listed because this is the region where encounter with entrained prey are most often initiated [21, 22, 47]. Fluid is entrained along the bell margin at maximum velocities of 6 cm s^{-1} and total shear rates of 0.50 s^{-1}. These values varied little among replicate medusae ($\sim$ 10%).

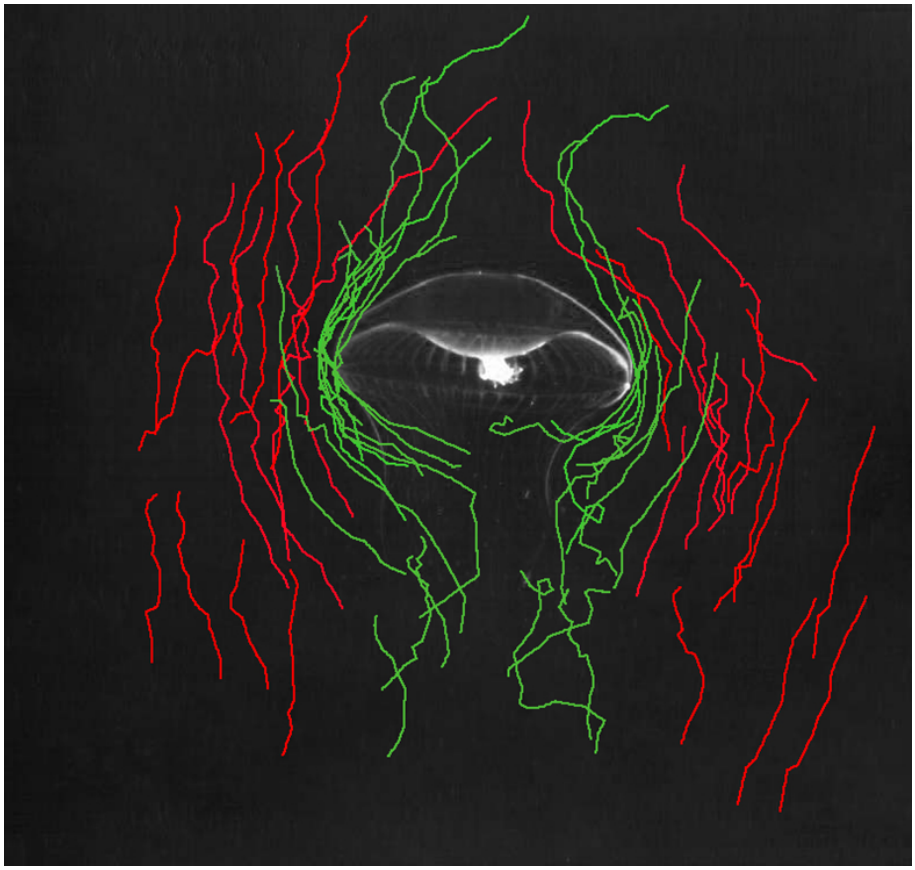

Figure 3.2. Prey tracks around *Aequorea victoria* in the laboratory. Green prey tracks indicate prey that are entrained and encountered (or passes through tentacles). Red prey tracks indicate prey not encountered by the medusae.

Table 3.2. Summary of relevant fluid and LCS parameters from laboratory (mean ± std. dev., $n = 5$) and field PIV measurements of flow surrounding *Aequorea victoria*.

	Maximum animal diameter (cm)	Distance per swim cycle (cm)	Duration per swim cycle (s)	Maximum marginal velocity (cm s^{-1})	Maximum marginal vorticity (s^{-1})	Maximum marginal shear (s^{-1})	Upstream LCS lobe area (cm^2)	Upstream LCS lobe volume (cm^3)	Prey encounter rate (L hr^{-1})
In vitro	5.56 ± 0.29	3.07 ± 0.24	0.69 ± 0.02	6.12 ± 0.62	0.37 ± 0.04	0.50 ± 0.02	1.22 ± 0.20	21.96 ± 2.39	11.43 ± 1.12
In situ	2.78	2.34	1.07	0.73	0.44	2.38	0.42	1.99	0.67

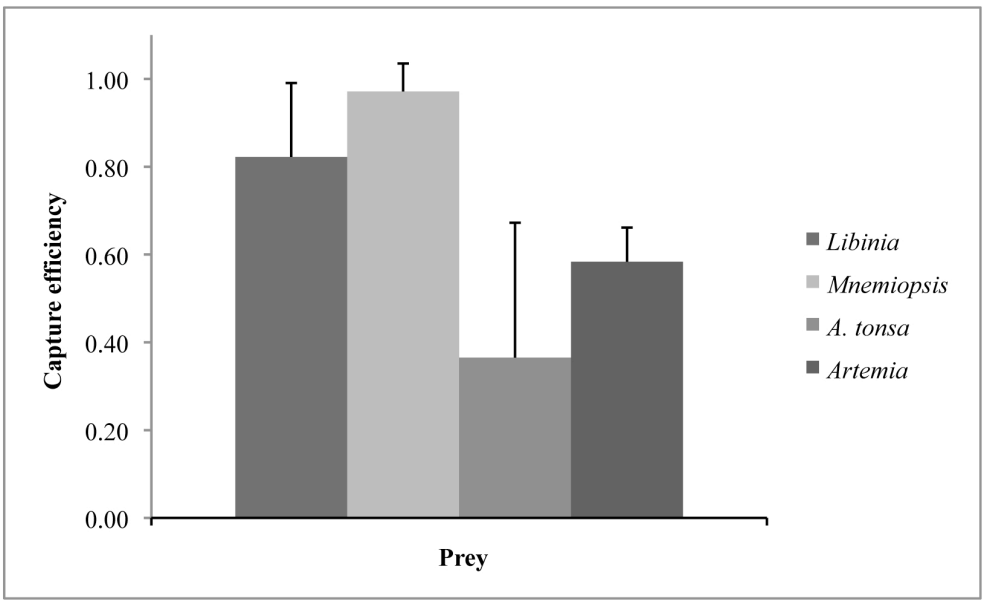

Figure 3.3. Variation of capture efficiency with prey type. Soft-bodied prey (*Libinia emarginata* and *Mnemiopsis leidyi*) have a higher capture efficiency than hard-bodied prey (*Artemia salina* and *Acartia tonsa*). Error bars denote standard deviation values in the measurement.

3.3.3 Lagrangian Analysis of Flow

The FTLE fields identify regions of convergent (attracting FTLE) and divergent (repelling FTLE) flow. Based on these regions we can identify discrete packets of fluid in front of the swimming medusa that will be encountered (i.e., transported through the capture surfaces). Figure 3.7 illustrates how the FTLE fields identify convergent and divergent regions in the flow. Two representative FTLE ridges (indicated by black boxes in figure 3.7A) are identified as potential LCS because LCS correspond to ridges (or local maxima) in the FTLE field [115]. These potential LCS are redrawn relative to the animal body in figure 3.7B (black curves). The red and blue asterisks identify actual particle pairs located on both sides of the attracting and repelling LCS. The position of these particle pairs is subsequently tracked through time (figure 3.7C). As predicted by the LCS, the position of particles on either side of an attracting or repelling LCS converge or diverge.

Starting earlier in the swim sequence, we visually identified regions of flow in front of the swimming *Aequorea victoria* by following the criteria for LCS extraction of a vortex ring [113, 84], whereby, the intersections of attracting and repelling ridges of FTLE fields (figure 3.8A) yield the LCS that

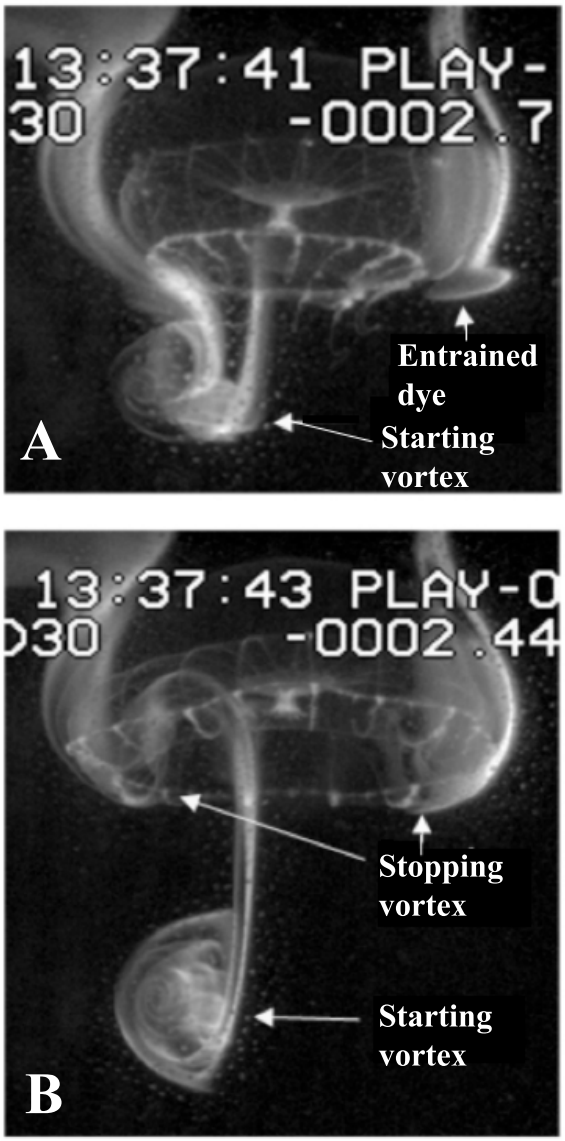

Figure 3.4. Visualization of flow around *Aequorea victoria* swimming in the laboratory using fluorescent dye. During bell contraction (A; maximum bell contraction shown), the starting vortex is formed; during expansion (B; maximum expansion shown), the stopping vortex is formed inside the subumbrellar cavity.

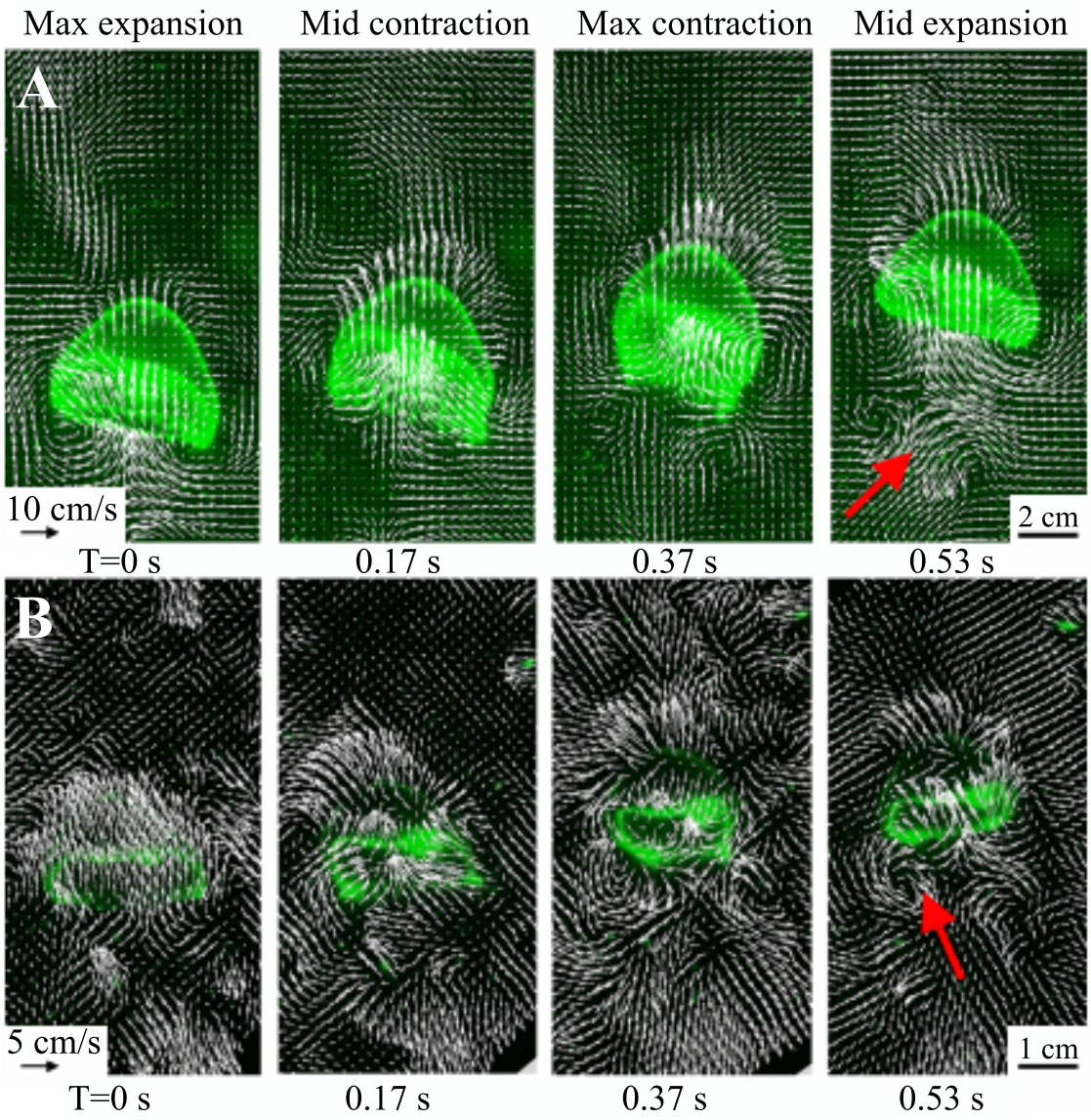

Figure 3.5. Velocity vectors from DPIV analysis around *Aequorea victoria* swimming in the laboratory (A) and natural field setting (B). Red arrows indicate vortex rings in the animals wake.

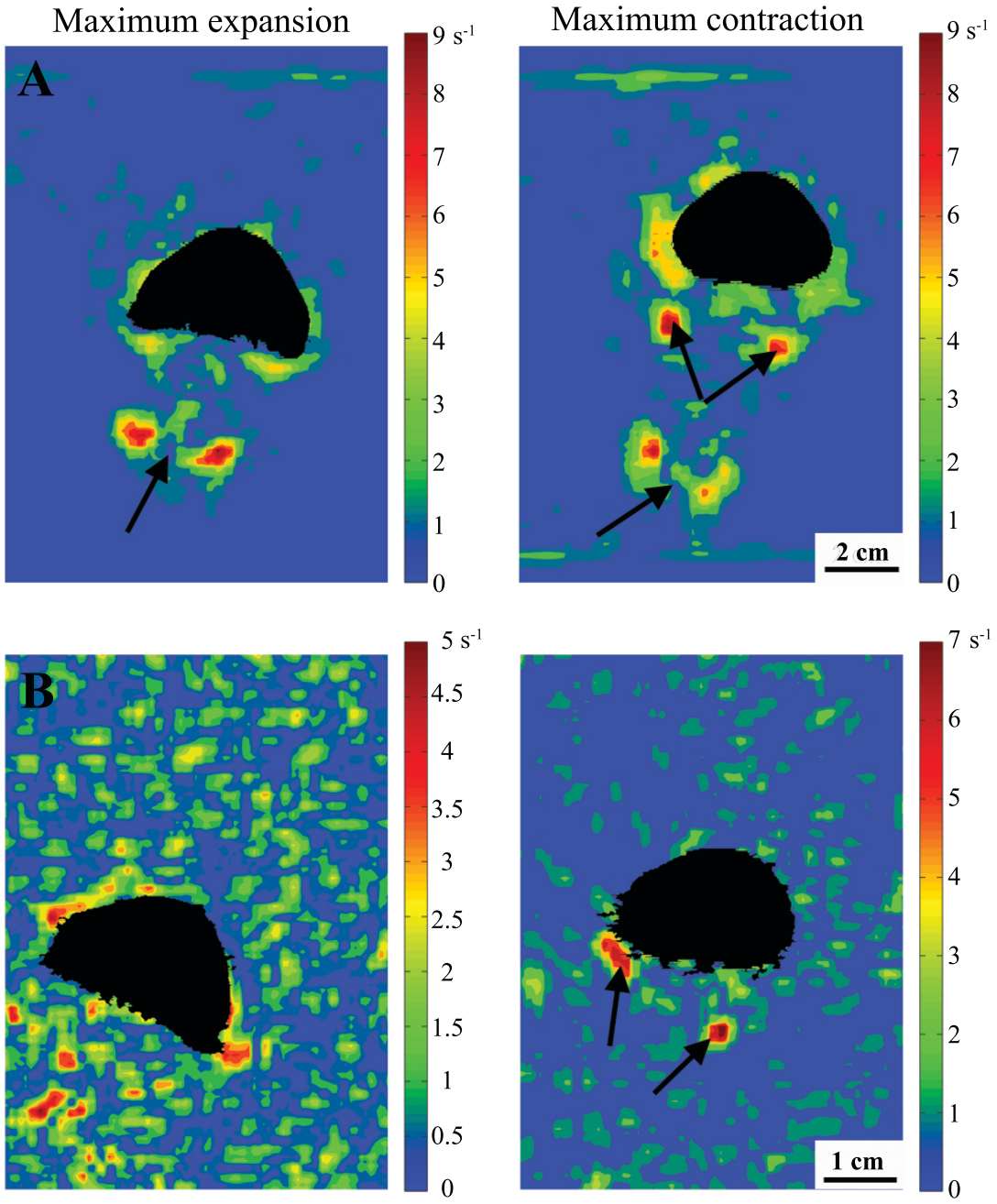

Figure 3.6. Magnitude of total shear rate (computed from equation (3.1)) around *Aequorea victoria* swimming in the laboratory (A) and natural field setting (B) at maximum expansion (left column) and maximum contraction (right column). Black arrows indicate vortex rings and vortex ring cores.

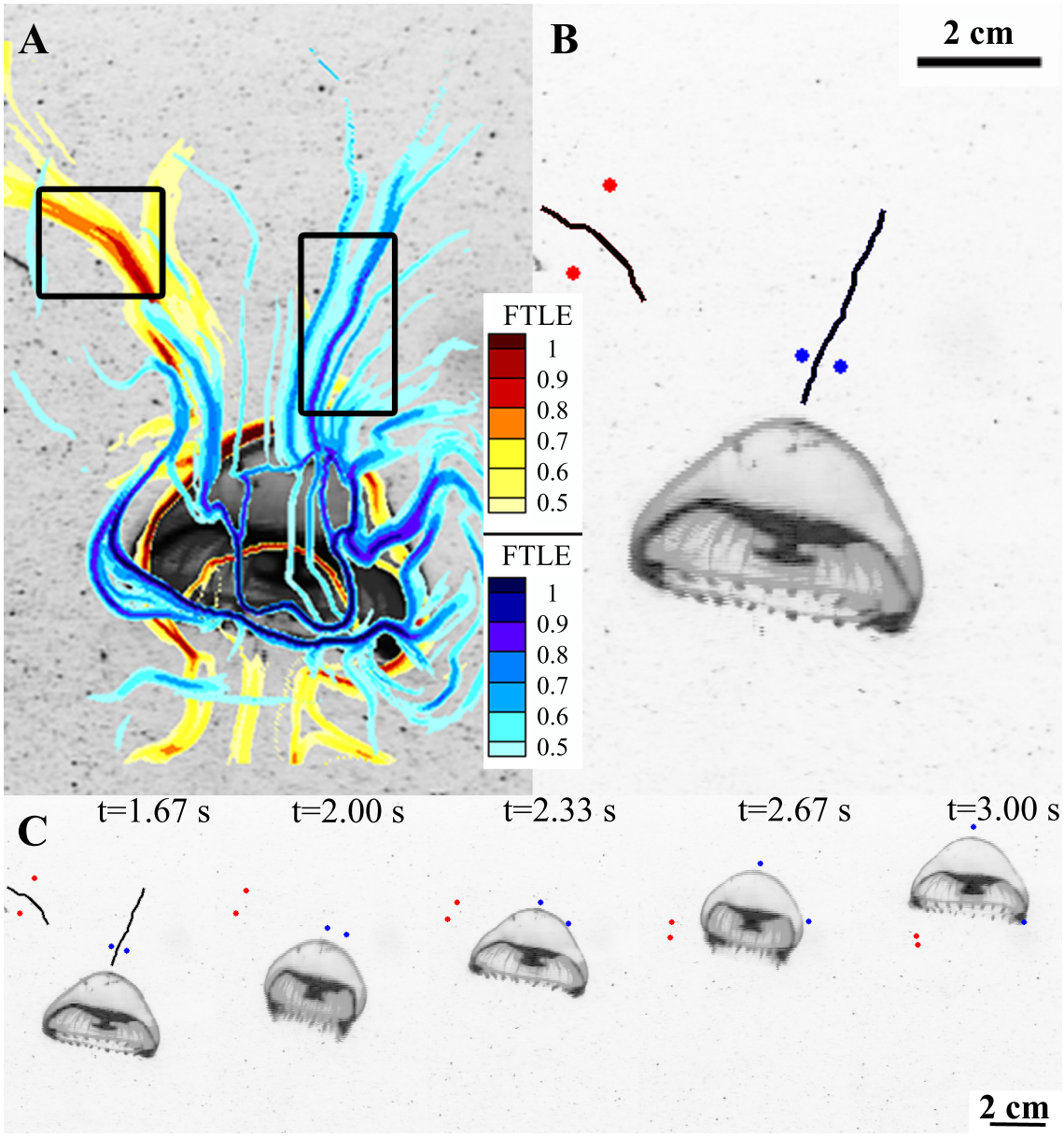

Figure 3.7. Laboratory FTLE field (computed using integration time $|T| = 60$ frames), extracted LCS curves, and the behavior of particles neighboring the curves as time is advected forward. A, The FTLE field corresponds to time $t = 1.67$ s. Ridges of the blue and red contours correspond to repelling (forward-time, $T > 0$) and attracting (backward-time, $T < 0$) LCS, respectively. B, Two potential attracting and repelling LCS curves are shown by the black curves and are indicated by the black boxes on the FTLE field (A). Blue and red dots show actual particles that are initially adjacent to and separated from each other on opposite sides of the attracting and repelling LCS curves, respectively. C, As time is advected forward, the distance between blue and red particles is increased and decreased, respectively.

bounds the animal (identified by the black line; figure 3.8B). The fluid inside the LCS lobe structures located upstream of the swimming animal indicate finite regions of fluid that will be brought into the oral region of the medusae occupied by the tentacles (identified as encountered fluid). Similar to figure 3.3, this figure shows that only discrete regions of fluid in front of swimming *Aequorea victoria* were entrained through these regions occupied by tentacles. We can approximate the volume of fluid an animal has the potential to interact with by a cylinder whose diameter and height is the animal diameter and distance traveled in a swimming cycle, respectively. From estimates of encountered fluid volume using LCS analysis (see section 3.2 and table 3.2), we see that *Aequorea victoria* entrains only 29.4% of the total 'cylinder' of fluid through which the medusan bell passes during a single swimming cycle. The subsequent transport of the encountered fluid is tracked through time in the wake of the swimming medusa (red packets of particles; figure 3.8C). The advection of particles in the flow of swimming animals is similar to traditional particle tracking techniques, however we are able to predict regions of fluid that interact with the animal a priori due to the LCS analysis. As particles are advected forward in time, their position relative to the LCS remain the same (red markers remain inside and blue markers remain outside the LCS) since LCS are material lines [115]. In addition, we see that particles located inside upstream lobes (red markers) are entrained into vortex rings that are generated in the animal's wake. Consequently, this enables us to use these LCS structures to determine flow that is entrained and encountered by the medusae as it swims.

To examine the effects of integration time T on the structure of LCS, we compared analyses based on integration times of 60 and 30 frames of data for the swimming sequence seen in figures 3.7A and 3.8A (and compared in figure 3.9). This is important because in some instances only a limited amount of video footage is available for analysis, thereby limiting the integration time (e.g., the field observations). The lobe structures adjacent to the animal body are more pronounced and numerous with longer integration times ($|T| = 60$ frames; figure 3.9A) than when using shorter integration times ($|T| = 30$ frames; figure 3.9B). Consequently, the number of upstream LCS lobes decrease as the integration time is reduced (figure 3.10B compared to figure 3.8B). These observations are consistent with previous published works [112, 105]. Despite these differences, the general structure

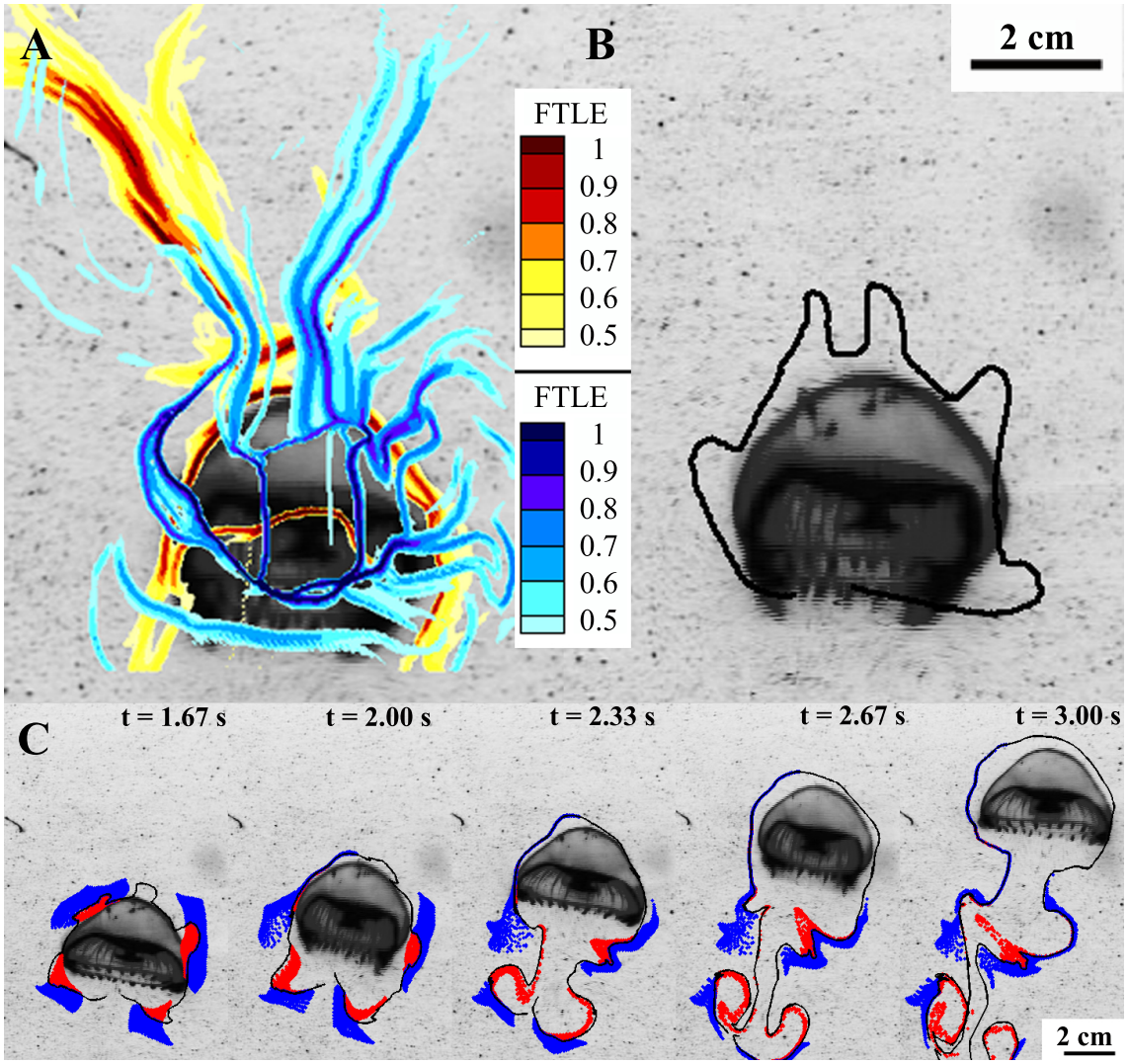

Figure 3.8. Extraction of LCS surrounding the animal body from the laboratory FTLE field and the position of marked particles relative to the LCS curve as time is advected forward. A, the FTLE field at time $t = 1.37$ s was found using an integration time of $|T| = 60$ frames. Blue and red contours correspond to repelling (forward-time, $T > 0$) and attracting (backward-time, $T < 0$) FTLE, respectively. Ridges of the FTLE field are potential LCS curves and the intersections of repelling and attracting FTLE yield a single LCS curve that surrounds the animal body (B, black curve). C, red and blue particles are initially located inside and outside the upstream LCS lobes, respectively. A series of images starting at time $t = 1.67$ s with an increment of 0.33 s between consecutive images shows the evolution of particle positions relative to the LCS as time is advected forward.

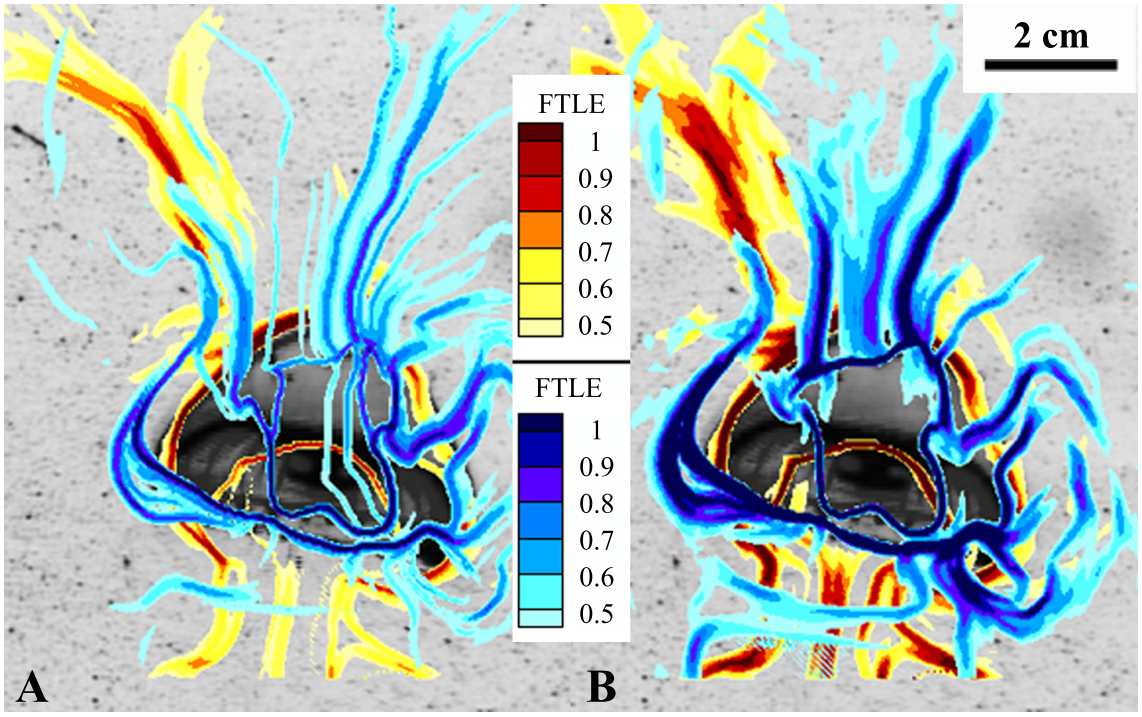

Figure 3.9. Comparison of laboratory FTLE fields at time $t = 1.67$ s using integration time $|T| =$ 60 frames (A) and $|T| = 30$ frames (B). Blue and red contours correspond to repelling (forward-time, $T > 0$) and attracting (backward-time, $T < 0$) FTLE, respectively.

of the flow remains the same, and we observe particles initially located inside the upstream LCS lobes are entrained into vortex rings in the animal's wake.

3.3.4 Analysis of In Situ Fluid Interactions

Both the in situ velocity vector fields (figure 3.5B) and shear fields (figure 3.6B) reveal the complexity of ambient flow surrounding medusae in natural field settings. To estimate how these ambient flow structures affect fluid transport by medusae, we collected a sequence of continuous swimming in the field. However, the data collected is only sufficient for LCS analysis at shorter integration times ($|T| = 30$ frames). As mentioned previously, shorter integration times may produce a less-refined picture of LCS boundaries than longer integration times. Nonetheless, the analysis is informative for illustrating the influence of ambient flows on the structure of the flows around swimming medusae. Using the criteria of Mathur et al. and Haller [84, 53], we confirm the presence of attracting and repelling LCS in the ambient fluid. The location of LCS (indicated by black and

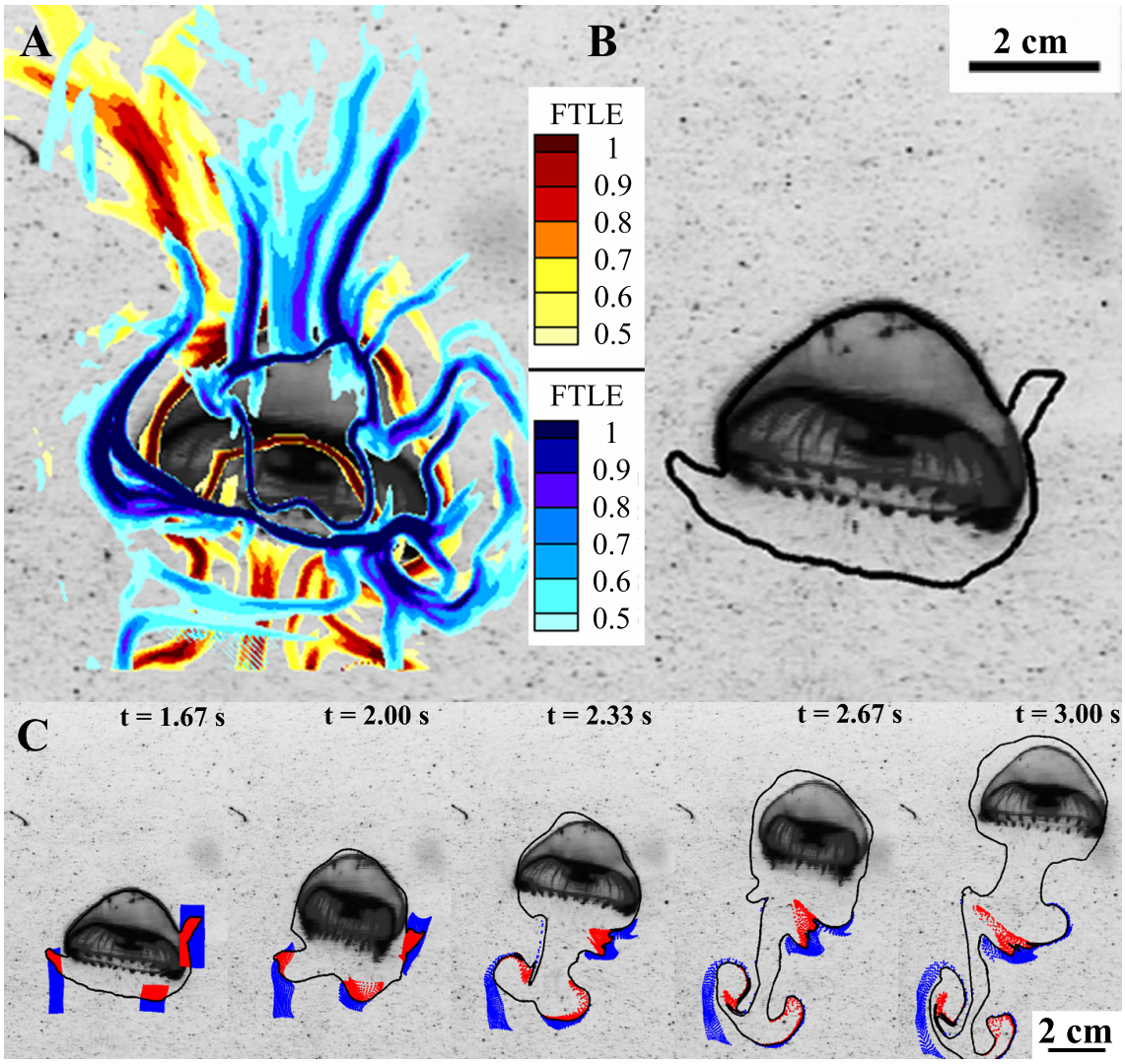

Figure 3.10. Extraction of LCS surrounding the animal body from the laboratory FTLE and the position of particles relative to the LCS curve as time is advected forward using an integration time of $|T| = 30$ frames. A, The FTLE field is at time $t = 1.67$ s. Blue and red contours correspond to repelling (forward-time, $T > 0$) and attracting (backward-time, $T < 0$) FTLE, respectively. Ridges of the FTLE field are potential LCS curves and the intersections of repelling and attracting FTLE yield a single LCS curve that surrounds the animal body (B, black curve). C, Red and blue particles are initially located inside and outside the upstream and downstream LCS lobes, respectively. A series of images starting at time $t = 1.67$ s with an increment of 0.33 s between consecutive images shows the evolution of particle position relative to LCS as time is advected forward.

white circles in figure 3.11) corresponds to attracting and repelling LCS. We see a strong interaction of maximal FTLE contours adjacent to the animal and maximal FTLE contours in the ambient fluid (figure 3.12). Physically, this means that the ambient flow generates regions of strong particle separation and attraction independent of *Aequorea victoria*'s feeding currents. An attracting FTLE ridge (or potential LCS, indicated by black boxes in figure 3.12A) is redrawn relative to an attracting LCS that is adjacent to the animal body (red curve, figure 3.12B), and illustrates how background flow structures interact with structures that dictate animal transport while swimming. As time is advected forward, the LCS found in the ambient fluid later attaches to the LCS that bounds the animal body. As an animal swims and encounters background flow in the ambient fluid environment, they interact with these flow structures, which results in the combining or separating of LCS from the animal body.

The presence of active flow structures in the surrounding fluid and their interaction with swimming medusae likely result in altered fluid transport compared to still water in filming vessels. Using the same LCS extraction criteria as before, the intersections of attracting and repelling ridges of FTLE fields (figure 3.13A) yield the LCS that bounds the animal but excludes the LCS in the ambient flow (figure 3.13B). The extracted LCS is identified by the black curve (figure 3.13B) and its deformation with time is also shown (figure 3.13C). Red and blue markers are initially placed inside and outside upstream and downstream LCS lobes, respectively. As in the laboratory case, red and blue particles remain inside and outside the bounding LCS, respectively (figure 3.13C). However, particles initially located inside the upstream LCS lobes (red markers) are not necessarily entrained in the vortex rings present in the animal wake.

3.4 Discussion

DPIV measurements of flow around swimming *Aequorea victoria* confirm the findings of previous qualitative studies that examined flow and feeding by *Aequorea victoria* and other oblate cruising-foraging medusae [21, 22, 47, 18, 57]. Maximum flow velocities were observed in regions adjacent to the bell margin and in trailing vortices. This flow has been shown to entrain and transport prey to

the capture surfaces of the medusae [22, 47, 57]. However, the maximum marginal flow velocities we observed (table 3.2) were more than two times greater than other similarly-sized medusae from studies using less quantitative methods [21, 18]. This has important implications for feeding because marginal flow velocity is thought to be an important parameter in determining prey selection by cruising-foraging medusae, such that prey with slower escapes speeds than the entraining flow are more likely to be captured than faster-escaping prey such as copepods [21]. Our observed marginal flow velocities are below many reports of copepod escape velocities [139, 11], however they are greater than some reports [122, 134]. Consequently, some copepods may have difficulty escaping entrainment and transport to capture surfaces. In addition, the levels of shear observed along the bell margin were also below the deformation rates that elicit escape responses from several copepods [69, 51, 11], suggesting that many copepods can be entrained into capture zones before detecting the medusa. However, shear levels in the vortices rotating through the tentacles reach levels at or above many copepod thresholds. Therefore, it would be possible for copepods to be entrained in medusan feeding currents but detect the predator and attempt an escape before contacting a tentacle [69, 51, 11]. However, the strength of vortices generated in the wake of *Aequorea victoria* may prevent escape of prey in encountered fluid regions as they pass through trailing tentacles, improving rates of predation. These finding suggest that copepods may be more vulnerable to predation by cruising-foraging medusae than previously thought. This vulnerability is consistent with observations of interactions between copepods and cruising-foraging medusae [122, 123] and some gut content data [124, 5].

The LCS analysis enables us to identify structures in the flow and determine how much fluid is transported through the tentacles of *Aequorea victoria* and the locations from which the flow originated. Similar to previous analyses on another cruising forager, *Aurelia aurita* [113, 96], the LCS analysis demonstrates that as *Aequorea victoria* swims it transports fluid from in front of its bell, along the regions immediately adjacent to the bell margin, and circulates the fluid into the trailing wake. These general characteristics are observed regardless of whether the analysis is performed over long (figure 3.8) or short integration times (figure 3.10). In addition, as was observed

for *Aurelia aurita*, only discrete packets of fluid are entrained into the wake that actually circulates through the tentacles of the medusa. Consequently, it appears that many cruising-foraging medusae may only interact with patches of fluid that their bells travel through, creating a mosaic of fluid that can be encountered. These similarities between *Aequorea victoria*, a hydromedusa, and *Aurelia aurita*, a scyphomedusa, support the notion that cruising-foraging medusae transport fluid similarly regardless of evolutionary origins [19, 24]. However, depending upon the placement of capture surfaces (such as tentacles and oral arms) different species would encounter different mosaics of fluid and create persistent structures in the wake (i.e., recirculation regions for *Aurelia* and vortex rings for *Aequorea*), which may enhance capture efficiency.

Quantitative characteristics of the LCS analysis can provide valuable estimates of how much fluid is transported through the tentacles of *Aequorea victoria*. Based on the LCS lobe volume compared to the cylinder of fluid that the bell of *Aequorea victoria* passes through, we estimate a 30% probability that prey upstream of a swimming medusae will be encountered. The volume of the LCS lobe divided by the swimming cycle time provides an estimate of the maximum clearance rate (F_{max}). Based on these assumptions, clearance rates of laboratory *Aequorea victoria* of 11.5 L hr^{-1} are reported (table 3.2). These numbers are consistent with previously published results on multiple species of comparably sized cruising medusae [129]. Weight-specific clearance rates for *Aequorea* based on laboratory LCS analysis was found to be 27 L gWW^{-1}, which is within the range reported for *Aequorea aequorea* in Prince William Sound, Alaska [101]. To our knowledge, weight-based clearance rates for *Aequorea victoria* have not been quantified until now. These values used in conjunction with capture and ingestion efficiencies could prove valuable for mechanistically-based predation models of cruising-foraging medusae.

The extracted LCS from field measurements (figure 3.13B) provided a comparison of laboratory data with an in situ data set. The field data is limited to a single animal, yet provides insight into how flow around foraging medusae may be influenced by natural flow conditions. The presence of background flow is apparent in the in situ velocity and shear fields (figures 3.5B and 3.6B). This flow appears to distort and redistribute upstream LCS lobes unevenly on either side of the animal,

creating asymmetric flow characteristics and fluid transport. In addition, vortex ring structures in the wake of in situ *Aequorea victoria* lack coherent shape. As a result, the size of the LCS lobes entrained by the medusae was reduced by $\sim$ 50% (occupying 14% versus 30% of the cylinder of fluid through which the bell interacts). However, during calm periods in the natural field setting, background flow structures dissipate, revealing similar vortical wake structures observed in the laboratory but at a slightly weaker signal (figure 3.5B, $t = 0.57$ s). These effects on fluid structure shape and location suggest that medusae may have less control over fluid and prey transport in a natural field setting than under quiescent flows in the laboratory. However, the overall effect on encounter is difficult to predict since turbulence is known to enhance predator-prey encounter rates [83]. Further, high shear in ambient flow is of the same order of magnitude as shear generated by a swimming predator (figure 3.6B). This may make medusae less detectable to prey, and hence, prey become more vulnerable to predation. Consequently, while the field data is currently limited, the LCS approach with in situ data does provide an approach for future studies by demonstrating that ambient flows may alter patterns of fluid entrainment by medusae and influence the detection of medusan predators by their prey.

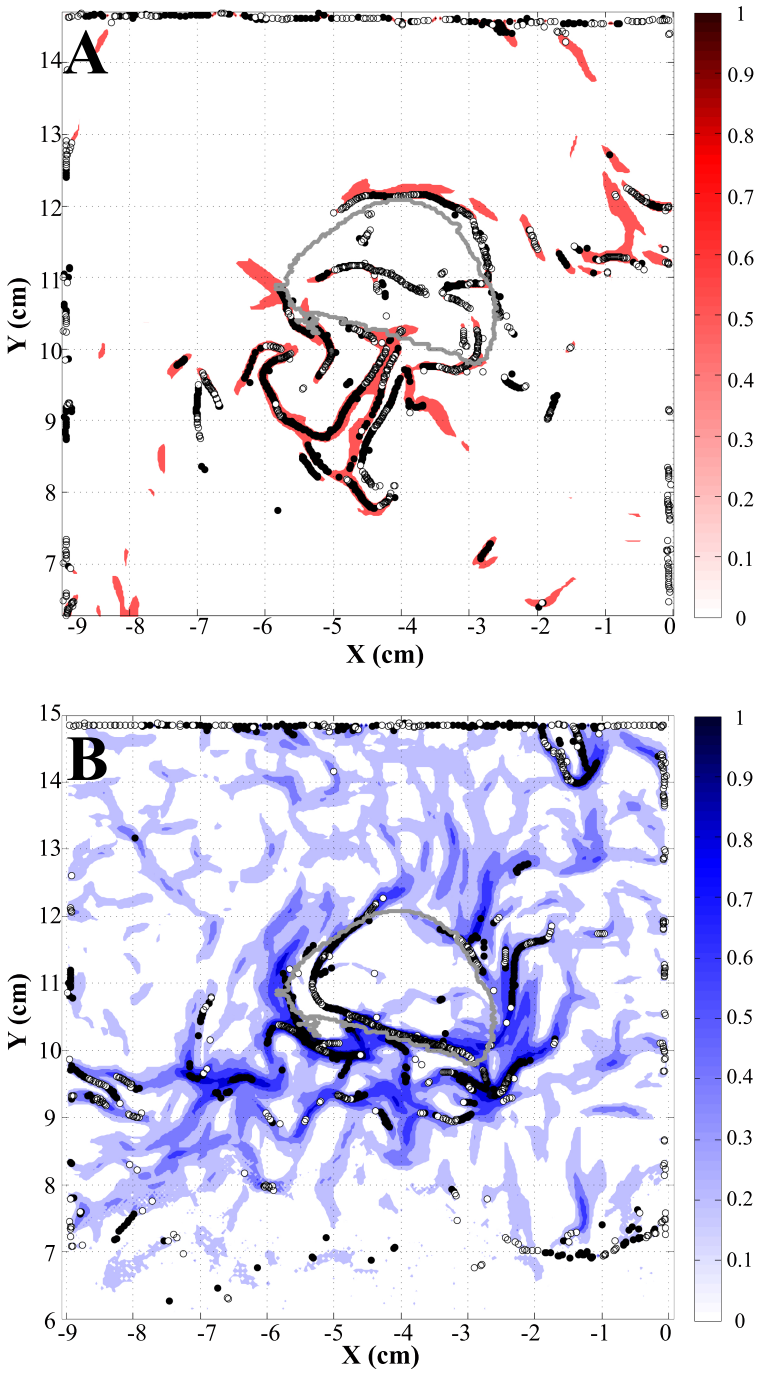

Figure 3.11. Identification of LCS from FTLE ridges using the criteria of Mathur et al. and Haller [84, 53]. Panels show the FTLE field and LCS (black and white circles) for the backward- (A, red contours) and forward-time (B, blue contours) computations. The outline of the animal body is indicated by the gray line. The location of LCS in the FTLE field correspond to attracting and repelling LCS.

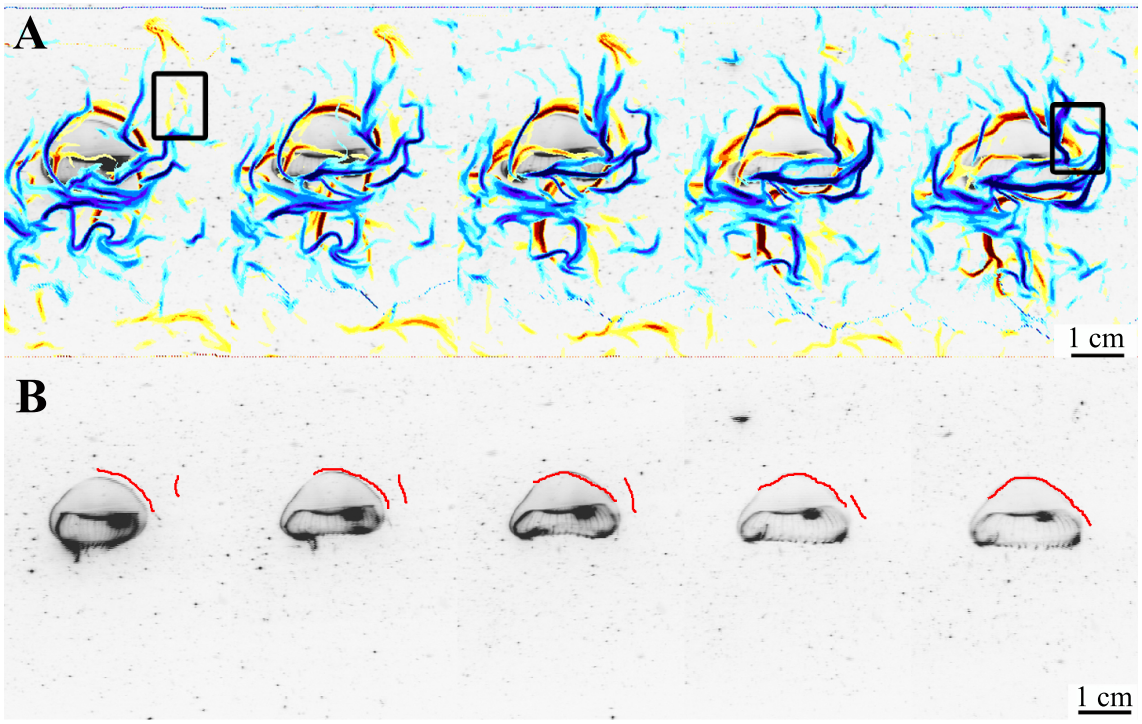

Figure 3.12. Time series of in situ FTLE fields and the position of an ambient attracting LCS relative to an LCS curve bound on the animal body. Both FTLE and LCS image series start at time $t = 3.00$ s with an increment of 0.17 s. Blue and red contours correspond to repelling (forward-time, $T > 0$) and attracting (backward-time, $T < 0$) FTLE, respectively. The black box in A highlights the starting and ending position of an attracting FTLE contour and is indicated by the red line that is initially separated from the animal body in B.

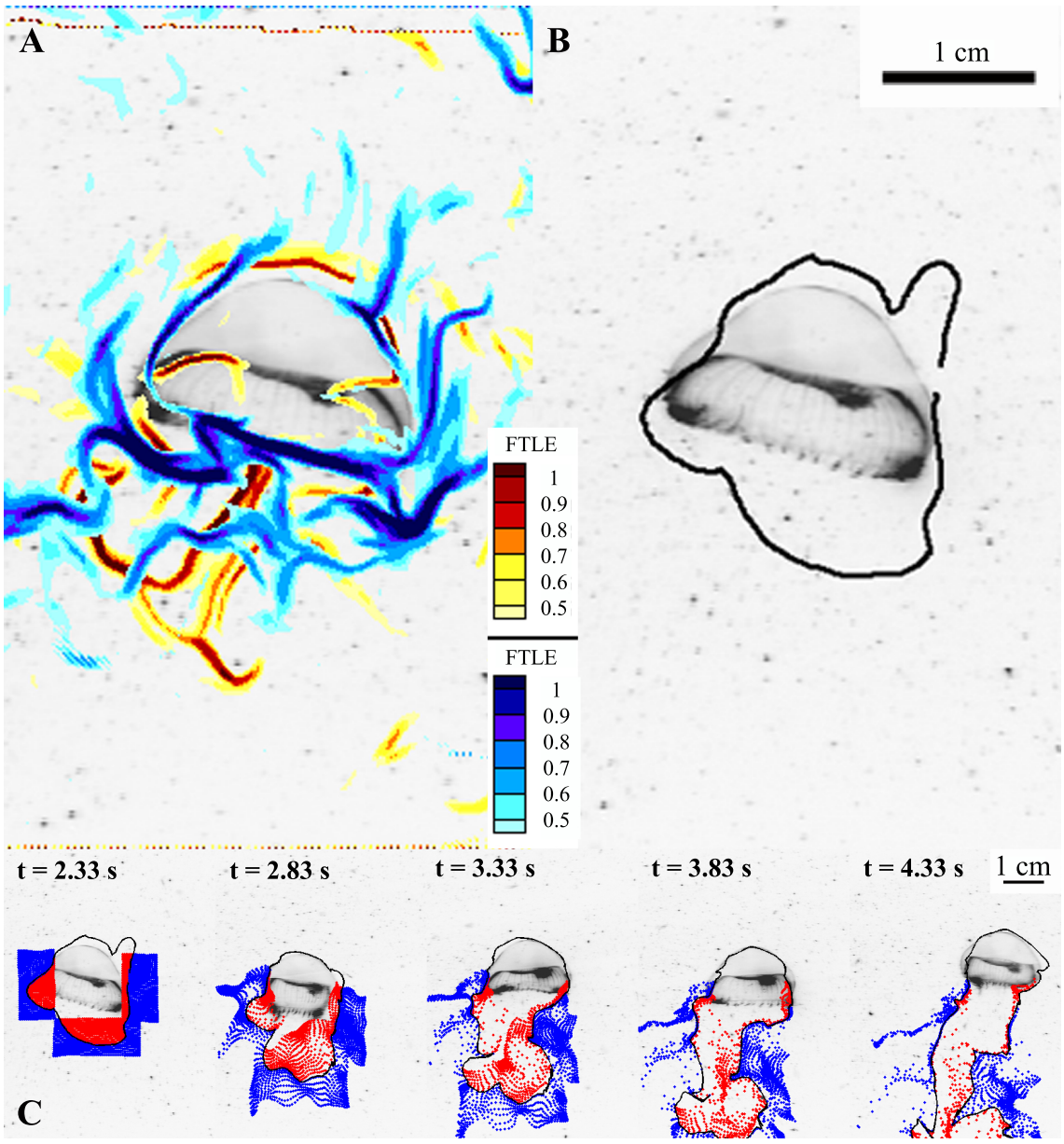

Figure 3.13. Extraction of LCS surrounding the animal body from the in situ FTLE field and the position of particles relative to the LCS curve as time is advected forward. A, The FTLE field at time $t = 2.33$ s was found using an integration time of $|T| = 30$ frames. Blue and red contours correspond to repelling (forward-time, $T > 0$) and attracting (backward-time, $T < 0$) FTLE, respectively. Ridges of the FTLE field are potential LCS curves and the intersections of repelling and attracting FTLE yield a single LCS curve that surrounds the animal body (B, black curve). C, Red and blue particles are initially placed inside and outside the upstream and downstream LCS lobes, respectively. A series of images starting at time $t = 2.33$ s with an increment of 0.5 s between consecutive images shows the evolution of particle position relative to LCS as time is advected forward.